

# Origin of chaos near three-dimensional quantum vortices: A general Bohmian theory

Athanasios C. Tzemos,<sup>\*</sup> Christos Efthymiopoulos,<sup>†</sup> and George Contopoulos<sup>‡</sup>

*Research Center for Astronomy and Applied Mathematics of  
the Academy of Athens Soranou Efessiou 4 Athens, GR-11527*

(Dated: November 6, 2018)

## Abstract

We provide a general theory for the structure of the quantum flow near 3-d ‘nodal lines’, i.e. one-dimensional loci where the 3-d wavefunction becomes equal to zero. In suitably defined coordinates (co-moving with the nodal line) the generic structure of the flow implies the formation of 3-d quantum vortices. We show that such vortices are accompanied by nearby invariant lines of the co-moving quantum flow, called ‘X-lines’, which are normally hyperbolic. Furthermore, the stable and unstable manifolds of the X-lines produce chaotic scatterings of nearby quantum (Bohmian) trajectories, thus inducing an intricate form of the quantum current in the neighborhood of each 3-d quantum vortex. Generic formulas describing the structure around 3-d quantum vortices are provided, applicable to an arbitrary choice of 3-d wavefunction. We also give specific numerical examples, as well as a discussion of the physical consequences of chaos near 3-d quantum vortices.

---

<sup>\*</sup> thanasitzemos@gmail.com

<sup>†</sup> cefthim@academyofathens.gr

<sup>‡</sup> gcontop@academyofathens.gr

## I. INTRODUCTION

The dynamics of quantum systems with vortices is of both theoretical and experimental interest. Quantum vortices are generated around singular points of the complex wavefunction  $\Psi$  and have been found in different physical problems with two or more dimensions [1, 2], e.g. field theory [3], Bose-Einstein condensates [4], decoherence theory [5], chemical reaction dynamics [6], wave-packet interference [7], quantum tunneling [8], molecular dynamics simulations [9, 10], electron microscopy [11], superconductors [12, 13] etc.

The trajectory-based, or ‘Bohmian’, approach [14–19] lends itself conveniently to the study of quantum vortices. In this approach, we consider trajectories which trace the quantum-mechanical currents according to the nonlinear (‘pilot-wave’) equations of motion. The trajectories are ”guided” by the wave-function  $\Psi$  which evolves in time according to the usual Schrödinger’s equation. The ‘ontological’ content of the Bohmian theory, as well as the ‘reality’ of Bohmian trajectories, has been a matter of intense debate over the years, in view also of its connection to experimental results or the interpretations of the results of statistical experiments (see for example [20–25]). On the other hand, a quite distinct motivation for studying the properties of Bohmian trajectories stems from the standpoint of applications of the *trajectory methods* in the quantum dynamics of particular physical systems (see [1] or [18, 19]). In fact, trajectory-based methods are useful in a variety of applications. In particular, the behavior of the trajectories close to quantum vortices presents special interest, since it has been demonstrated that trajectories scattered by quantum vortices exhibit complex or *chaotic* behavior. The connection of chaos with the existence of nodal points of the wavefunction has been established since long [26–34]. Besides its general importance in all the above mentioned applications, chaos plays a special role in the accuracy of methods aiming to compute the Schrödinger evolution through quantum trajectories, as, for example, in hydrodynamical solvers of the Schrödinger equation [35, 36], or in the conditional wave function approach to the quantum N-body problem [37–39]. Finally, as reviewed in [40], chaos may play a crucial role in a more theoretical framework, i.e., the question of how the rules of quantum probabilities (Born’s rule) can be shown to emerge through the statistical properties of quantum trajectories [41, 42] (see also [22, 43]).

Regarding, now, the mechanisms which lead to the emergence of chaotic Bohmian trajectories in the presence of quantum vortices, in 2005 Wisniacki and Pujals and Borondo et

al. (see [30, 44]) were the first to emphasize that it is the motion of quantum nodes which is responsible for the generation of chaos. In ([30, 44]) the emergence of chaos is described by the mechanism of homoclinic tangle. In [33], analytical formulas are provided showing that the emergence of a ‘nodal point-Xpoint’ topology close to any node is general, i.e. it applies for arbitrary choices of quantum model and wavefunction, while chaos is described as a ‘scattering’ phenomenon. The connection of the scattering phenomenon with the homoclinic approach ([30, 44]) is an open problem.

The mechanisms of chaos discussed in ([30], [44]) and [33] refer to 2-d quantum systems. To our knowledge no such study of the mechanism of chaos has yet been presented in the case of three dimensional systems. This is, precisely, our scope in the present work.

In our work below we establish generic formulas which hold for the description of the quantum flow close to *nodal lines*, i.e. one dimensional curves representing continuous families of nodal points in the 3-d configuration space. These formulas justify theoretically results found in specific numerical examples in two previous papers of ours [45, 46]. The key remark, originally due to [29], is that in the neighborhood of a nodal line, the quantum flow is arranged in a foliation of surfaces which are nearly planar and normal to the nodal line. Following [29], these are called below the ‘Falsaperla-Fonte planes’, or simply ‘F-planes’. Since sufficiently close to a nodal point the quantum flow becomes essentially planar (i.e. nearly confined in a F-plane), the generic picture found in [33] for vortices in 2-d systems can be generalized in the 3-D case as well, with a number of additional considerations (or terms, in the formulas) accounting for the distortion of the quantum flow with respect to a perfectly planar form.

According to this picture, the projection of the quantum flow in the F-plane around every nodal point along one nodal line takes the form shown schematically in Fig.1. This figure illustrates the quantum flow in the F-plane as viewed in a frame of reference *co-moving with a nodal point*. We find that every nodal point is necessarily accompanied by a single second critical point of the comoving flow, called ‘X-point’, whose linear stability character is hyperbolic. In the rest frame, this is a point in space where the quantum trajectory has instantaneous velocity equal to that of the nodal point. The whole structure, as viewed in the co-moving frame, is called a ‘nodal point-X-point complex’ (NPXPC). Taking the foliation of all NPXPCs along a nodal line forms a ‘3-d structure of NPXPCs’. This structure complements in a substantial way the ‘cylindrical structure’ observed in [45],

by adding a continuous family of X-points to it, which we call the ‘X-line’. This is a one-dimensional critical curve of the flow as viewed in a frame co-moving with the nodal line (see precise definitions in section II and Appendix I). As such, the ‘X-line’ constitutes a normally hyperbolic manifold [47], wherefrom 2-dimensional unstable and stable manifolds emanate. As shown below, one branch of these manifolds terminates in the nodal line through spirals, while the remaining branches asymptotically deviate away from the X-line.

The so-formed 3-d structure gives a complete characterization of the 3-d quantum vortex around a nodal line. More importantly, trajectories which come close to the X-line undergo hyperbolic scattering with features similar to those described in [33] for the 2-D case. As a result, the local value of the Lyapunov exponent (or ‘stretching number’ [48, 49]) undergoes positive jumps in every such scattering, hence accumulating to a positive Lyapunov characteristic exponent, i.e., chaos. This latter result is verified by numerical experiments, as described in section III, hence validating the theory of section II below.

The paper is structured as follows: in section II we develop the general theory of the structure of the quantum flow (and trajectories) near quantum vortices, supplemented with a generic set of formulas which apply for arbitrary 3-d wavefunctions possessing nodal lines. In section III we validate the theoretical analysis of the previous section by numerical experiments, computing a real (non-schematic) example of ‘the 3-d structure of NPXPCs’, and probing the correlation between jumps in the local Lyapunov exponents of trajectories and close encounters with the X-line. Section IV summarizes the basic conclusions of the present study.

## II. 3-D STRUCTURE OF NODAL AND X POINTS: GENERAL THEORY

### A. Summary of results

Consider a 3-d quantum system with wavefunction  $\Psi(x, y, z, t)$ , at the time  $t$ , where  $(x, y, z)$  are Cartesian space co-ordinates. The quantum current is given by  $\mathbf{j} = \frac{\hbar}{2mi}(\Psi^*\nabla\Psi - \Psi\nabla\Psi^*)$  ( $\hbar$  = Planck’s constant,  $m$  = the particle mass,  $\hbar = m = 1$  in the sequel). The quantum current can be traced by a swarm of ‘Bohmian’ trajectories defined via the flow  $\mathbf{v} = \mathbf{j}/|\Psi|^2$ . These equations of motion take the generic form

$$\frac{dx}{dt} = f_x(x, y, z, t), \quad \frac{dy}{dt} = f_y(x, y, z, t), \quad \frac{dz}{dt} = f_z(x, y, z, t) \quad . \quad (1)$$

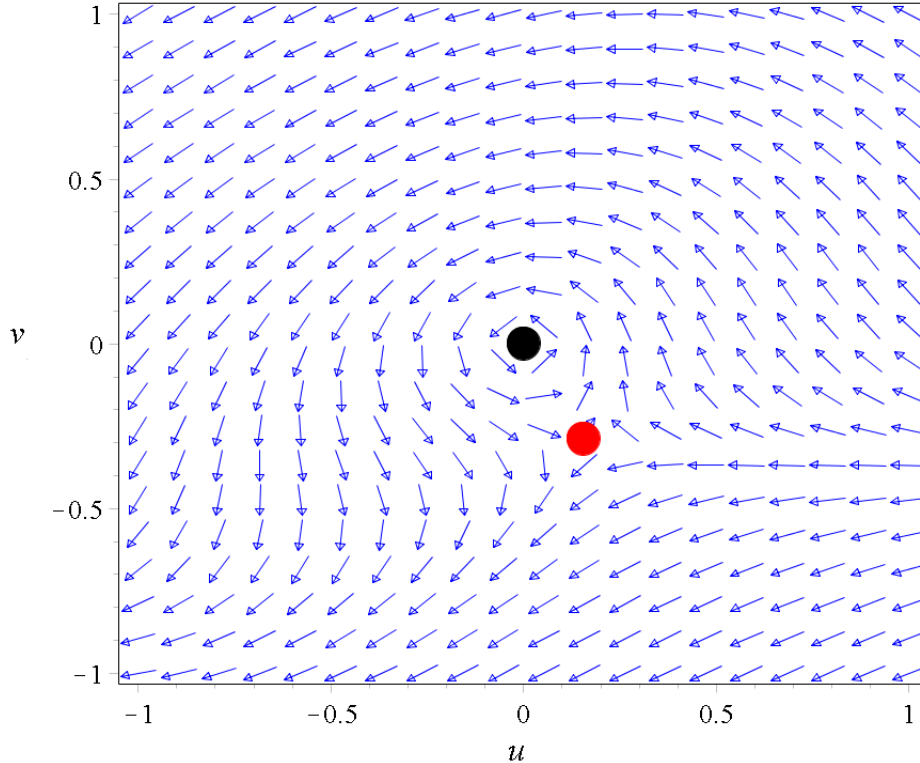


FIG. 1: The local quantum flow on the F-plane around a nodal point. In coordinates co-moving with the nodal point, the flow very close to the nodal point (black dot) has the shape of a spiral, while further away there is an X-point (red dot) which has zero velocity with respect to the nodal point.

Eqs.(1) constitute a non-autonomous 3-d dynamical system. Numerical investigations in various systems of the form (1) have revealed the typical existence of chaotic trajectories (see, for example [27, 29, 45]). Our purpose is to explain the dynamical origin of the trajectories' chaotic behavior. To this end, it proves crucial to focus on the structure of the flow induced by Eqs.(1) near loci in space where  $\Psi(x, y, z, t) = 0$ . These loci are the 'nodal lines' of the wavefunction  $\Psi$ .

We invoke the following two approximations, further specified in subsequent sections:

i) Under an appropriate 'adiabatic' condition (see subsection II E), the flow (1) in a neighborhood of every point along a nodal line, and within a given time interval, can be approximated as nearly autonomous in a set of variables  $(u, v, w)$ , found after a linear transformation  $\mathcal{L} : (x, y, z) \rightarrow (u, v, w)$ . The variables  $(u, v, w)$  correspond physically to co-ordinates locally

attached to and co-moving with each separate nodal point along a nodal line.

ii) One can use the above co-ordinates in order to construct a new dynamical system of the form:

$$\frac{dU}{d\tau} = F_U(U, V, S), \quad \frac{dV}{d\tau} = F_V(U, V, S), \quad \frac{dS}{d\tau} = F_S(U, V, S) \quad (2)$$

where the variables  $(U, V, S)$  are provided by a transformation

$$(U, V, S) = (u, v, w) + \mathcal{NL}(u, v, w) \quad (3)$$

$\mathcal{NL}(u, v, w)$  being a small nonlinear correction to the identity. The new time  $\tau$  corresponds to a suitably defined re-parametrization of the original time  $t$ .

Using the above approximations, we deduce the following, which is the main result of the present paper: We show that the equations of motion (2) admit as solution an invariant continuous family of hyperbolic points, which, together, form a normally hyperbolic ‘X-line’. Furthermore, the stable and unstable manifolds of the X-line connect with the associated nodal line through a family of spirals, forming a 3-d vortex. This we call the ‘3-d structure of nodal point - X-point complexes’. The geometric structure of these manifolds serves to explain the hyperbolic scattering of nearby trajectories, i.e., the appearance of chaos near 3-d quantum vortices. In particular, it is the dynamics close to the X-line, rather than close to the nodal line, which is responsible for chaos. This latter fact is substantiated with numerical experiments in section III.

The complete construction of the transformation (3), as well as the Eqs.(2), is given in Appendix I. Most features of these equations can be approximated by a local construction, which yields equations of motion around only one nodal point along a nodal line. We now focus on the latter construction, which is similar as the one introduced in [33] for 2-d systems.

## B. Nodal line

Let  $\Psi_R(x, y, z, t) = \Re(\Psi(x, y, z, t))$ ,  $\Psi_I(x, y, z, t) = \Im(\Psi(x, y, z, t))$ . We assume that, at fixed time  $t$ , the  $2 \times 3$  set of equations

$$\Psi_R(x, y, z, t) = 0, \quad \Psi_I(x, y, z, t) = 0 \quad (4)$$

admits solutions lying in one or more curves in the space  $(x, y, z)$ . We call such curves the ‘nodal lines’ of the wavefunction  $\Psi$  at the time  $t$ .

Depending on the wavefunction under study, the shape of nodal lines at a given time  $t$  can be quite complex, as it can be composed of different branches, possibly forming loops or extending to infinity. On the other hand, it is possible to introduce a continuous parametrization of one nodal line in every open segment of it. To this end, let  $O$  be an arbitrary point along a nodal line not belonging to its boundary (we call  $O$  the ‘origin’). In an open neighborhood  $\mathcal{V}_0$  of  $O$ , we define  $s$  to be the length parameter along the curve, starting from  $O$  and with sign indicating the direction of inscription of the line with respect to  $O$ . For every point of the nodal line  $(x_0, y_0, z_0)$  belonging to  $\mathcal{V}_0$  we can then assign a unique value of  $s$ , thus defining the continuous and smooth functions  $x_0(s), y_0(s), z_0(s)$ .

Setting  $\Psi = \Psi_R + i\Psi_I$ , the Bohmian equations of motion in the inertial frame read (with  $m = \hbar = 1$ ):

$$\mathbf{v} = \dot{\mathbf{r}} = \frac{\Psi_R \nabla \Psi_I - \Psi_I \nabla \Psi_R}{\Psi_R^2 + \Psi_I^2}. \quad (5)$$

Since  $\Psi_R(x_0(s), y_0(s), z_0(s), t) = \Psi_I(x_0(s), y_0(s), z_0(s), t) = 0$  one has

$$\frac{d\Psi_R}{ds} = \nabla \Psi_R \cdot \frac{d\mathbf{r}_0}{ds} = 0, \quad \frac{d\Psi_I}{ds} = \nabla \Psi_I \cdot \frac{d\mathbf{r}_0}{ds} = 0 \quad (6)$$

and, hence,  $\nabla \Psi_R \perp d\mathbf{r}_0/ds$ ,  $\nabla \Psi_I \perp d\mathbf{r}_0/ds$  at all points  $\mathbf{r}_0 \equiv (x_0, y_0, z_0)$ . Then, by Eq.(5) we deduce that the Bohmian velocity field tends to become normal to the nodal curve as we tend towards any point on this curve. The plane normal to a nodal curve at one of its nodal points is called the ‘F-plane’ associated with the nodal point (see [29]).

Assuming the wavefunction to be continuous and with continuous derivatives in  $\mathcal{V}_0$  at all times between  $t$  and  $t + \Delta t$ , where  $\Delta t$  is a small time interval, Eqs.(4) imply that the nodal line evolves smoothly in time within  $\mathcal{V}_0$ . In particular, let  $\mathcal{F}_{\mathbf{r}_0, t}$  be the F-plane associated with the nodal point  $\mathbf{r}_0$  at the time  $t$ , and  $\mathbf{r}_0(t')$  be the point where the nodal line at a later time  $t'$  intersects the same F-plane  $\mathcal{F}_{\mathbf{r}_0, t}$ , for all  $t'$  with  $t \leq t' \leq t + \Delta t$ . We define the velocity  $\mathbf{V}_0$  of the nodal point  $\mathbf{r}_0$  at the time  $t$  as

$$\mathbf{V}_0(t) = \lim_{t' \rightarrow t} \frac{\mathbf{r}_0(t') - \mathbf{r}_0(t)}{t' - t}. \quad (7)$$

Clearly, the velocity vector  $\mathbf{V}_0(t)$  belongs to  $\mathcal{F}_{\mathbf{r}_0, t}$ , thus it is also perpendicular to the nodal line.

We note here that, as it will be discussed below, ‘X-lines’ necessarily appear only when we consider the quantum flow around *time-varying* nodal lines. Similarly to the 2-d case (see [32, 33]), in order to describe this phenomenon we must consider the form of the quantum

flow in a co-ordinate frame co-moving with the nodal line. In turn, this requires assigning a value of the velocity to every point along the nodal line. However, contrary to the 2-d case, in the 3-d case such assignment cannot be done unambiguously on the sole basis of the shape evolution of the nodal line at nearby times, since there are infinitely many ways to continuously map each point of the nodal line, at time  $t$ , to a point on the deformation of the same nodal line at a later time  $t' > t$ . Using the intersection of the nodal line with the F-plane  $\mathcal{F}_{\mathbf{r}_0,t}$  allows to bypass this ambiguity.<sup>1</sup>

### C. Structure of the flow near nodal points: quantum vortices

Let  $\mathbf{r}_0 = (x_0, y_0, z_0)$  be a particular nodal point at the time  $t = t_0$ . We now consider a coordinate change  $(x, y, z) \rightarrow (u, v, w)$  such that: i)  $(x_0, y_0, z_0) \rightarrow (0, 0, 0)$ , i.e. the node is at the origin, ii) the new co-ordinates are such that the  $w$ -axis is tangent to the nodal line at the point  $(x_0, y_0, z_0)$ , while the  $u$  and  $v$  are directions in the associated F-plane defined via a pre-selected geometric rule. For example, if  $\mathbf{t}$ ,  $\mathbf{n}$ ,  $\mathbf{b}$  are the tangent, normal and bi-normal unitary vectors of the nodal line at  $\mathbf{r}_0$ , for an arbitrary point  $\mathbf{r} \equiv (x, y, z)$  we define the transformation (Fig. 2):

$$u = \Delta\mathbf{r} \cdot \mathbf{n}, \quad v = \Delta\mathbf{r} \cdot \mathbf{b}, \quad w = \Delta\mathbf{r} \cdot \mathbf{t} \quad (8)$$

where  $\Delta\mathbf{r} = \mathbf{r} - \mathbf{r}_0$ . Since Eqs.(8) become singular at points  $\mathbf{r}_0$  where the curvature of the nodal line becomes zero, we can use, alternatively, the transformation:

$$\begin{pmatrix} u \\ v \\ w \end{pmatrix} = \begin{bmatrix} \sin \phi_m & -\cos \phi_m & 0 \\ \cos \theta_m \cos \phi_m & \cos \theta_m \sin \phi_m & -\sin \theta_m \\ \sin \theta_m \cos \phi_m & \sin \theta_m \sin \phi_m & \cos \theta_m \end{bmatrix} \begin{pmatrix} x - x_0 \\ y - y_0 \\ z - z_0 \end{pmatrix} \quad (9)$$

with

$$\phi_m = \arctan(t_y/t_x) \quad (10)$$

$$\theta_m = \arccos(t_z/|t|) \quad (11)$$

---

<sup>1</sup> One may also remark that the Bohmian equations (5) cannot be used directly to define  $\mathbf{V}_0(t)$ , since the r.h.s. of these equations are singular at  $\mathbf{r} = \mathbf{r}_0$  at the time  $t$ .



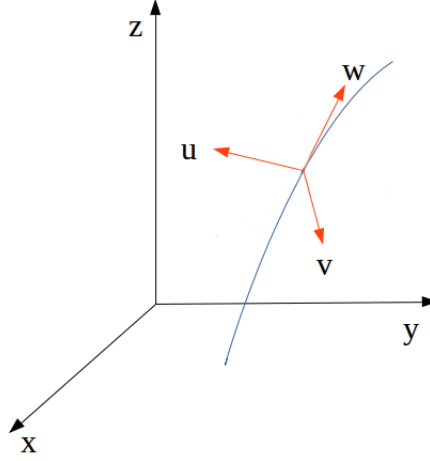


FIG. 2: Inertial (black) and moving (red) frames of reference. The axis  $\mathbf{w}$  is tangent locally to the nodal line (blue curve), while the axes  $\mathbf{u}, \mathbf{v}$  lie in the F-plane.

where  $\mathbf{t} = (t_x, t_y, t_z)$ . Equations (9) become singular whenever  $\mathbf{t}$  becomes parallel to the  $z$ -axis. In numerical simulations we use both (8) and (9), ensuring to properly deal with the corresponding singularities.

Expressing  $\Psi$  in the new co-ordinates  $\Psi \equiv \Psi(u, v, w, t)$ , Eqs.(4) and (6) take the form

$$\Psi(0, 0, 0, t = t_0) = 0, \quad \left. \frac{\partial \Psi}{\partial w} \right|_{u=0, v=0, w=0, t=t_0} = 0$$

Then, Taylor-expanding  $\Psi$  around the origin (the nodal point) and up to terms of second degree in the variables  $u, v, w$  yields

$$\begin{aligned} \Psi = & a_{000} + (a_{100} + ib_{100})u + (a_{010} + ib_{010})v + (a_{200} + ib_{200})u^2 + (a_{020} + ib_{020})v^2 \\ & + (a_{002} + ib_{002})w^2 + (a_{110} + ib_{110})uv + (a_{101} + ib_{101})uw + (a_{001} + ib_{001})vw + \dots \end{aligned} \quad (12)$$

with real *time-dependent* coefficients  $a_{ijk}(t)$ ,  $b_{ijk}(t)$ ,  $i, j, k = 0, 1, \dots$ . One has  $a_{000}(t_0) = 0$ . As in the corresponding analysis in the 2-d case (see [33]), we now consider a frame of reference centered at the nodal point  $\mathbf{r}_0$  and moving with uniform velocity  $(V_u, V_v, V_w)$  equal to the instantaneous velocity  $\mathbf{V}_0$  of the nodal point defined in Eq.(7). Setting  $G = \Psi_R^2 + \Psi_I^2 =$

$(a_{100}u + a_{010}v)^2 + (b_{100}u + b_{010}v)^2 + \dots$ , the equations of motion in the above frame read

$$\begin{aligned}\frac{du}{dt} &= \frac{1}{G} \left[ \left( \frac{\partial \Psi_I}{\partial u} \Psi_R - \frac{\partial \Psi_R}{\partial u} \Psi_I \right) - V_u G \right] \\ \frac{dv}{dt} &= \frac{1}{G} \left[ \left( \frac{\partial \Psi_I}{\partial v} \Psi_R - \frac{\partial \Psi_R}{\partial v} \Psi_I \right) - V_v G \right] \\ \frac{dw}{dt} &= \frac{1}{G} \left[ \left( \frac{\partial \Psi_I}{\partial w} \Psi_R - \frac{\partial \Psi_R}{\partial w} \Psi_I \right) - V_w G \right].\end{aligned}\tag{13}$$

We have  $V_w = 0$ , since, by definition, the velocity  $\mathbf{V}_0$  is orthogonal to the nodal line. We also note that the r.h.s. of Eqs.(13) depends explicitly on time through the time dependence of the wavefunction  $\Psi$ .

Due to Eq.(12), we readily find that, as  $\Psi \rightarrow 0$  at  $t = t_0$ , the numerators in the r.h.s. of the first two of the Eqs.(13) tend to zero by terms linear in  $u, v$ , while the denominator (equal to  $G$ ) tends to zero by terms quadratic in  $u, v$ . Thus, at  $t = t_0$ , the velocities  $du/dt, dv/dt$  in Eqs.(13) tend to infinity as we tend towards the nodal point  $\mathbf{r}_0$ . This implies that one can always find a sufficiently small neighborhood of the nodal point in which the Bohmian trajectories are inscribed with velocities much larger than  $\mathbf{V}_0$ . As in ([33]) we then invoke an *adiabatic approximation* to approximate Eqs.(13) as nearly autonomous, i.e., to ‘freeze’ the time in the r.h.s. of Eqs.(13) and replace the dynamical system (13) with

$$\begin{aligned}\frac{du}{dt} &= \left( \frac{1}{G} \left[ \left( \frac{\partial \Psi_I}{\partial u} \Psi_R - \frac{\partial \Psi_R}{\partial u} \Psi_I \right) - V_u G \right] \right)_{t=t_0} \\ \frac{dv}{dt} &= \left( \frac{1}{G} \left[ \left( \frac{\partial \Psi_I}{\partial v} \Psi_R - \frac{\partial \Psi_R}{\partial v} \Psi_I \right) - V_v G \right] \right)_{t=t_0} \\ \frac{dw}{dt} &= \left( \frac{1}{G} \left[ \left( \frac{\partial \Psi_I}{\partial w} \Psi_R - \frac{\partial \Psi_R}{\partial w} \Psi_I \right) - V_w G \right] \right)_{t=t_0}\end{aligned}\tag{14}$$

The exact conditions of validity of the above adiabatic approximation are similar to those established in [33] (see also subsection II E).

Under the approximation (14), the quantum flow in the moving frame of reference becomes singular for trajectories very close to the nodal point. However, such singularity is regularizable via a time transformation. Let  $(u(t), v(t), w(t))$  be a trajectory of Eqs.(13). Let  $t \rightarrow \tau$  be the time transformation defined via the differential equation  $d\tau/dt = G(u(t), v(t), w(t))$ . In the new time  $\tau$ , the trajectories of the system (13) are

given by the ‘reduced’ dynamical system

$$\begin{aligned}
\frac{du}{d\tau} &= \left( \frac{\partial \Psi_I}{\partial u} \Psi_R - \frac{\partial \Psi_R}{\partial u} \Psi_I \right) - V_u G \\
\frac{dv}{d\tau} &= \left( \frac{\partial \Psi_I}{\partial v} \Psi_R - \frac{\partial \Psi_R}{\partial v} \Psi_I \right) - V_v G \\
\frac{dw}{d\tau} &= \left( \frac{\partial \Psi_I}{\partial w} \Psi_R - \frac{\partial \Psi_R}{\partial w} \Psi_I \right).
\end{aligned} \tag{15}$$

We note, in particular, that the system (15) shares the same critical points and geometrical trajectories with the system (13), as can be deduced, e.g., by dividing each of the first two equations in (13) and (15) by the third equation respectively. Hereafter we work with the reduced equivalent dynamical system (15) which is devoid of infinities in the close neighbourhood of the nodal point. This improves significantly the precision of numerical calculations of trajectories, where we can implement time regularization in the integration scheme. Also, by freezing the new time  $\tau = \tau_0$  in the r.h.s. of Eqs.(15), one obtains the same approximate trajectories as in the system (14).

Returning to our analysis, the nodal point  $\mathbf{r}_0$ , i.e.,  $u_0 = v_0 = w_0 = 0$  becomes a stationary point of the quantum flow as represented in the ‘frozen time’ approximation of Eqs.(15). In the second order approximation, these equations (15) read:

$$\begin{aligned}
\frac{du}{d\tau} &= -Av + A_{200}u^2 + A_{020}v^2 + A_{002}w^2 + A_{110}uv + A_{011}vw + \dots \\
\frac{dv}{d\tau} &= Au + B_{200}u^2 + B_{020}v^2 + B_{002}w^2 + B_{101}uw + B_{110}uv + \dots \\
\frac{dw}{d\tau} &= C_{200}u^2 + C_{020}v^2 + C_{110}uv + C_{101}uw + C_{011}vw + \dots \quad ,
\end{aligned} \tag{16}$$

with

$$\begin{aligned}
A &= (a_{100}b_{010} - a_{010}b_{100}) \\
A_{011} &= (a_{010}b_{101} + a_{011}b_{100} - a_{100}b_{011} - a_{101}b_{010}) \\
A_{110} &= 2(a_{010}b_{200} - a_{200}b_{010}) - 2V_u(a_{100}a_{010} + b_{100}b_{010}) \\
A_{020} &= a_{010}b_{110} + a_{020}b_{100} - a_{100}b_{020} - a_{110}b_{010} - V_u(a_{010}^2 + b_{010}^2) \\
A_{002} &= (a_{002}b_{100} - a_{100}b_{002}) \\
A_{200} &= a_{100}b_{200} - a_{200}b_{100} - V_u(a_{100}^2 + b_{100}^2) \\
B_{200} &= a_{100}b_{110} - a_{110}b_{100} + a_{200}b_{010} - a_{010}b_{200} - V_v(a_{100}^2 + b_{100}^2) \\
B_{002} &= (a_{002}b_{010} - a_{010}b_{002})
\end{aligned}$$

$$\begin{aligned}
B_{020} &= a_{010}b_{020} - a_{020}b_{010} - V_v (a_{010}^2 + b_{010}^2) \\
B_{101} &= (a_{100}b_{011} - a_{011}b_{100} + a_{101}b_{010} - a_{010}b_{101}) = -A_{011} \\
B_{110} &= 2(a_{100}b_{020} - a_{020}b_{100}) - 2V_v (a_{100}a_{010} + b_{100}b_{010}) \\
C_{200} &= (a_{100}b_{101} - a_{101}b_{100}) \\
C_{020} &= (a_{010}b_{011} - a_{011}b_{010}) \\
C_{011} &= 2(a_{010}b_{002} - a_{002}b_{010}) = -2B_{002} \\
C_{101} &= 2(a_{100}b_{002} - a_{002}b_{100}) = -2A_{002} \\
C_{110} &= (a_{010}b_{101} - a_{101}b_{010} + a_{100}b_{011} - a_{011}b_{100})
\end{aligned}$$

where  $a_{ijk}, b_{ijk}$  are the coefficients of the wavefunction expansion (12) at the time  $t = t_0$ . We observe the basic symmetries  $A_{011} = -B_{101}, C_{101} = -2A_{002}, C_{011} = -2B_{002}$ .<sup>2</sup>

Linearization of the system (15) around the nodal point yields the equations

$$\frac{du}{d\tau} = -Av, \quad \frac{dv}{d\tau} = Au, \quad \frac{dw}{d\tau} = 0 \quad . \quad (17)$$

The eigenvalues of the associated Jacobian matrix are  $(iA, -iA, 0)$ . Thus, to the lowest order approximation, the nodal point is a nilpotent center of the flow. The eigenvector associated with the zero eigenvalue is  $(0, 0, 1)$ , which corresponds to a vector tangent to the

---

<sup>2</sup> We note that in quantum systems described by wavefunctions of the form:

$$\Psi(\mathbf{x}, t) = e^{\sigma(\mathbf{x})} \phi(\mathbf{x}, t)$$

where  $\sigma(\mathbf{x})$  a real-valued function, a more precise expansion of the equations of motion can be found:

$$\begin{aligned}
\dot{\mathbf{x}} &= \Im \left( \frac{\nabla \Psi(\mathbf{x}, t)}{\Psi(\mathbf{x}, t)} \right) = \frac{\nabla \Psi_I(x, t) \Psi_R(\mathbf{x}, t) - \nabla \Psi_R(x, t) \Psi_I(x, t)}{\Psi_R^2(x, t) + \Psi_I^2(\mathbf{x}, t)} \\
&= \frac{\nabla \phi_I(\mathbf{x}, t) \phi_R(\mathbf{x}, t) - \nabla \phi_R(\mathbf{x}, t) \phi_I(\mathbf{x}, t)}{\phi_R^2(\mathbf{x}, t) + \phi_I^2(\mathbf{x}, t)}
\end{aligned}$$

where  $\phi(\mathbf{x}, t) = \phi_R(\mathbf{x}, t) + i\phi_I(\mathbf{x}, t)$ . In such systems, one obtains the same formulas as in Eq.(16), where the coefficients  $a_{ijk}, b_{ijk}$  refer to the Taylor expansion, as in Eq.(12), but of the function  $\phi$  instead of  $\Psi$ . All symmetries of the coefficients and consequent results apply equivalently for the functions  $\phi$  and  $\Psi$ . In numerical computations, however, using the coefficients of  $\phi$  yields results more precise than those found with the coefficients of  $\Psi$ .

nodal line at the nodal point  $\mathbf{r}_0$ , while the center manifold of the system (17) coincides with the F-plane  $\mathcal{F}_0$ .

In the linear approximation, the trajectories in  $\mathcal{F}_0$  are circles described around the nodal point with frequency  $\omega = A$ . However, due to the fact that all eigenvalues have null real part, these linear solutions are not structurally stable with respect to nonlinear perturbations (see [50]). Thus, to determine the character of the trajectories we must consider higher than linear order terms of the system (16).

As in [33] we transform Eqs.(16) to cylindrical coordinates  $R, \phi, w$ , by setting  $u = R \cos \phi, v = R \sin \phi$ . This leads to a system of three ordinary differential equations which contain coupling terms polynomial in  $R, w$  and trigonometric polynomial in the azimuth  $\phi$ . Explicit solutions within a bounded domain around the nodal point  $\mathbf{r}_0$  can be constructed under the following approximations: assume the wavefunction  $\Psi$  has support over a volume in configuration space of linear size  $\mathcal{L}$ . Consider a sphere  $\mathcal{S}_\epsilon$  of radius  $\epsilon$  centered around the nodal point  $\mathbf{r}_0$ , where  $\epsilon$  is chosen such that, for all initial conditions within  $\mathcal{S}_\epsilon$ , the second-order truncation of the equations of motion (Eqs.(16)) yields solutions differing from the solutions of the complete system by less than a prescribed accuracy up to a maximum time of interest. Let now  $R_0$  be the radius of curvature of the nodal line at the point  $\mathbf{r}_0$ . Consider the open domain  $\mathcal{V}_\epsilon$  defined by all points within  $\mathcal{S}_\epsilon$  such that  $\mathcal{L}|w| < \epsilon^{3/2}R_0^{1/2}$ . It can be shown that, for all points within the domain  $\mathcal{V}_\epsilon$ , there are positive constants  $C_1 = \mathcal{O}(\mathcal{L}^{-9/2})$ ,  $C_2 = \mathcal{O}(\mathcal{L}^{-7/2})$  such that the following relations hold

$$\max(|a_{002}|, |b_{002}|) |w|^2 < C_1 \epsilon^3, \quad \max(|a_{002}|, |b_{002}|) |w| < C_2 \epsilon^{3/2} R_0^{-1/2}, \quad (18)$$

where  $a_{002}$  and  $b_{002}$  are the coefficients of the wavefunction expansion appearing in (12).<sup>3</sup> In normalized units ( $\mathcal{L} \sim 1$ ), the first of Eqs.(18) implies that, within the domain  $\mathcal{V}_\epsilon$ , every

---

<sup>3</sup> Assuming  $\mathbf{r}_0$  not to be an inflection point of the nodal line, the nodal line close to  $\mathbf{r}_0$  has the form of a parabola  $\gamma$ , which can be represented by a parametrization in terms of functions  $u_\gamma(w), v_\gamma(w)$  as:

$$u_\gamma(w) = \frac{1}{2}g_u w^2 + \mathcal{O}(w^3), \quad v_\gamma(w) = \frac{1}{2}g_v w^2 + \mathcal{O}(w^3),$$

with  $g_u = d^2 u_\gamma / dw^2|_{w=0}$ ,  $g_v = d^2 v_\gamma / dw^2|_{w=0}$ . One has  $g_u = \mathcal{O}(R_0^{-1})$ ,  $g_v = \mathcal{O}(R_0^{-1})$ . Using the above equation, as well as the Taylor expansion (12), Eq.(6) yields, to the lowest order (linear in  $w$ ), the set of equations:

$$2a_{002} + a_{100}g_u + a_{010}g_v = 0, \quad 2b_{002} + b_{100}g_u + b_{010}g_v = 0 \quad .$$

term containing a factor  $A_{002}w^2$  or  $B_{002}w^2$  in the first two of Eqs.(16) is of order  $\mathcal{O}(\epsilon^3)$ , while the remaining terms are of order  $\mathcal{O}(\epsilon^2)$ . Ignoring the terms  $A_{002}w^2$  or  $B_{002}w^2$ , and transforming to cylindrical co-ordinates, the first two of Eqs.(16) then take the form

$$\begin{aligned}\frac{dR}{d\tau} &= \frac{(u\dot{u} + v\dot{v})}{R} = c_2(\phi)R^2 + \dots \\ \frac{d\phi}{d\tau} &= \frac{(u\dot{v} - v\dot{u})}{R^2} = d_0 + d_1(\phi)R + h_1w + \dots\end{aligned}\quad (19)$$

where the coefficients  $c_2(\phi)$ ,  $d_1(\phi)$  are odd trigonometric functions of  $\phi$ ,  $d_0 = A = \text{const}$ , and  $h_1 = B_{101}$ . The last relation is a consequence of the symmetry  $A_{011} = -B_{101}$ , and plays a crucial role below. Finally, the third of Eqs.(16) takes the form

$$\frac{dw}{d\tau} = e_2(\phi)R^2 + k_2(\phi)Rw + \dots\quad (20)$$

where  $e_2(\phi)$  and  $k_2(\phi)$  are trigonometric functions of  $\phi$ , even and odd respectively.

Equations (19) and (20) still contain nonlinear couplings between the co-ordinates  $(R, \phi, w)$ , thus obstructing obtention of an explicit solution. As in [33], we then compute an ‘averaged’ system of equations which possesses an explicit solution. Dividing the first with the second of Eqs.(19), and averaging over the angle  $\phi$  we find the average dependence of  $R$  on  $\phi$  (denoted  $\bar{R}$ ) along the quantum flow in the neighborhood of  $\mathbf{r}_0$  as:

$$\frac{d\bar{R}}{d\phi} = \frac{1}{2\pi} \int_0^{2\pi} \left( \frac{c_2(\phi)R^2 + \dots}{d_0 + d_1(\phi)R + h_1w + \dots} \right) d\phi .$$

Expanding the denominator in the quantities  $d_1/d_0$ ,  $h_1/d_0$  and taking into account the parity and form of the various trigonometric coefficients defined above leads to

$$\frac{d\bar{R}}{d\phi} = \langle f_3 \rangle \bar{R}^3 + \dots\quad (21)$$

where

$$\langle f_3 \rangle = \frac{1}{2\pi} \int_0^{2\pi} \frac{1}{d_0} \left( -\frac{c_2 d_1}{d_0} \right) d\phi .$$

After some algebra we find

$$\langle f_3 \rangle = \frac{(A_{110} + 2B_{020})A_{020} + A_{200}(A_{110} - 2B_{200}) - B_{110}(B_{020} + B_{200})}{8A^2}\quad (22)$$

---

Restoring units ( $\Psi \sim \mathcal{L}^{-3/2}$ ), we find  $a_{002} = \mathcal{O}(\mathcal{L}^{-7/2}/R_0)$ ,  $b_{002} = \mathcal{O}(\mathcal{L}^{-7/2}/R_0)$ , which leads to the inequalities (18).

Moreover, for the average value of the angle  $\phi$  we get

$$\frac{d\bar{\phi}}{d\tau} \simeq A \Rightarrow \bar{\phi} = \phi_0 + A\tau \quad (23)$$

Thus we can write:

$$\frac{d\bar{R}}{d\tau} = \frac{d\bar{R}}{d\bar{\phi}} \frac{d\bar{\phi}}{d\tau} = \langle f_3 \rangle \bar{R}^3 A \quad (24)$$

which, upon integration, gives the average distance as a function of time:

$$\bar{R}(\tau) = \frac{R_0}{\sqrt{1 - 2R_0^2 \langle f_3 \rangle A \tau}} = \frac{R_0}{\sqrt{1 - 2R_0^2 \langle f_3 \rangle (\bar{\phi} - \phi_0)}} \quad (25)$$

Equation (25) allows to see that the projection of the orbit on the F-plane  $\mathcal{F}_0$  has the form of a spiral around the nodal point. In the forward sense of time, the spiral is inscribed counterclockwise (clockwise) if  $A > 0$  ( $A < 0$ ). Likewise, the nodal point acts as attractor, if  $\langle f_3 \rangle A < 0$ , or repeller, if  $\langle f_3 \rangle A > 0$ . Similarly to the 2-d case (see [32], [33]), *Hopf bifurcations* of limit cycles can take place at critical instances (of parameterized time  $\tau = \tau_c$ , or  $t = t_c$  in the original time) when  $\langle f_3 \rangle$  becomes equal to zero. Such limit cycles are generated at the nodal point, and they grow in radius away from, and surrounding, the nodal point, for times close to  $t_c$ .

We note, that in special models such as the one of [30, 44], the Bohmian flow takes a conservative form which implies that the node acts as a center and  $\langle f_3 \rangle$  is always equal to zero. In this case, as established in [30, 44], one finds chaos close to the nodes due to the existence of a homoclinic tangle. An interesting question regards the connection of homoclinic theory with the mechanism of chaos discussed in [33] and in the present paper, which is based on the scattering of Bohmian trajectories close to the nodal points (see section III below).

The evolution in the third dimension, normal to the F-plane  $\mathcal{F}_0$  can now be approximated by substituting the ‘averaged’ solutions  $\bar{R}(\tau)$ ,  $\bar{\phi}(\tau)$  of Eqs.(25) and (23) into Eq.(20). Then

$$w(\tau) = w_0 + \exp \left( \int_0^\tau d\tau' k_2 (\bar{\phi}(\tau')) \bar{R}(\tau') \right) \times \int_0^\tau d\tau' \left[ e_2 (\bar{\phi}(\tau')) \bar{R}^2(\tau') \left( \exp \left( - \int_0^{\tau'} d\tau'' k_2 (\bar{\phi}(\tau'')) \bar{R}(\tau'') \right) \right) \right] \quad (26)$$

The full 3-d geometric shape of the trajectories is helical, as one can see from the averaged equation

$$\frac{d\bar{w}}{d\phi} = \frac{1}{2\pi} \int_0^{2\pi} \left( \frac{e_2(\phi)R^2 + k_2(\phi)Rw + \dots}{d_0 + d_1(\phi)R + h_1w + \dots} \right) d\phi \quad .$$

To the lowest approximation we find

$$\frac{d\bar{w}}{d\bar{R}} = \frac{d\bar{w}}{d\bar{\phi}} \frac{d\bar{\phi}}{d\bar{R}} \approx \frac{\langle e_2 \rangle}{\langle f_3 \rangle A \bar{R}}$$

with solution

$$\bar{w}(\bar{R}) \approx w_0 + \frac{\langle e_2 \rangle}{\langle f_3 \rangle A} \ln(\bar{R}/R_0) \quad . \quad (27)$$

Thus, a trajectory started at  $(R_0, \phi_0, w_0)$  inscribes a helix, keeping a spiral projection in the F-plane  $\mathcal{F}_0$  given by Eq.(25), while unfolding in the direction normal to  $\mathcal{F}_0$  according to the logarithmic envelope  $\bar{w}(\bar{R})$ , given by Eq.(27) (see Fig.3).

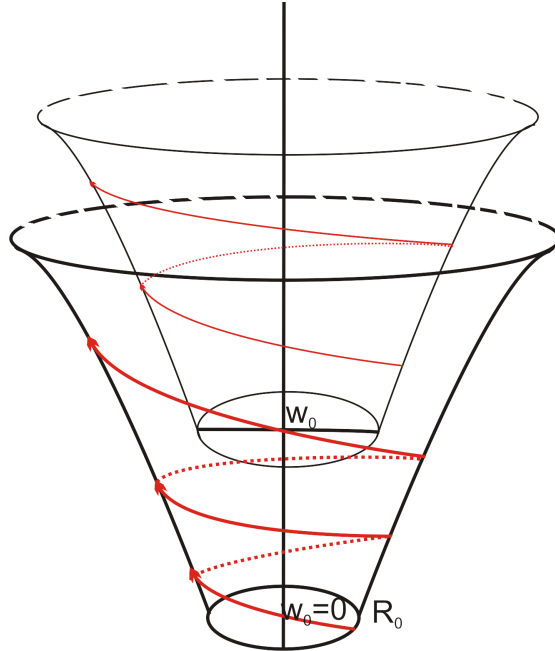


FIG. 3: Schematic representation of the trajectories in the neighborhood of one nodal point along a nodal line. The trajectories are helical and they lie in a foliation of conoidal surfaces of revolution, generated by the envelope curves given by Eq.(27) and parameterized by  $(R_0, w_0)$ .

Note that the two equations taken together, (25) and (27), define a foliation of cylindrical surfaces of revolution in which lie all helical trajectories parameterized by the different initial conditions  $(R_0, \phi_0, w_0)$ .



## D. X-point

An ‘X-point’ is defined as a critical point of the local quantum flow around a given nodal point, where the velocity of the trajectory in the inertial frame is equal to that of the nodal point. We find such points numerically using standard root-finding techniques. On the other hand, the existence, uniqueness (i.e. that only one X-point can be associated with the flow around each individual nodal point) and hyperbolic character (one real positive and one real negative eigenvalue of the linearized flow around the X-point) can be established in a similar way as in the 2-D case via the following approximations. We first require that the nodal point moves sufficiently fast so that the following inequality holds:

$$\max\{|V_u|, |V_v|\} \gg \frac{\max\{|a_{ijk}|, |b_{ijk}|, i + j + k = 2\}}{\min\{|a_{ijk}|, |b_{ijk}|, i + j = 1, k = 0\}}. \quad (28)$$

The condition (28) implies that the theory does not apply if the nodal point is stationary or moves slowly. As explained in detail below, this means that the scattering of the Bohmian trajectories, which leads to chaos, is a generic consequence of the fast motion of the nodal points. Thus, while counter examples can be found (see [34]), the generic mechanism leading to chaos is connected with moving nodes in the 3-d configuration space. Eqs.(16) yield

$$\frac{du}{d\tau} = -Av - G_2V_u + F_{u,2}, \quad \frac{dv}{d\tau} = Au - G_2V_v + F_{v,2}, \quad \frac{dw}{d\tau} = F_{w,2} \quad (29)$$

where  $G_2 = (a_{100}u + a_{010}v)^2 + (b_{100}u + b_{010}v)^2$ , while in view of the condition (28), the terms  $F_{u,2}, F_{v,2}, F_{w,2}$  can be disregarded as they are smaller in size than the maximum size of the terms  $G_2V_u, G_2V_v$ . For a second stationary point of the flow, denoted  $(u_X, v_X, w_X)$ , the r.h.s. of Eqs.(29) must become equal to zero. Then, taking into account Eq.(29), the following relation holds:

$$s_X \equiv \frac{v_X}{u_X} \simeq -\frac{V_u}{V_v}. \quad (30)$$

The approximation (30) can be used to obtain a sequence of approximants  $(u_X^{(r)}, v_X^{(r)}, w_X^{(r)})$  of the exact stationary point as follows: replacing first Eq.(30) into the last of Eqs.(16) with  $\frac{dw}{dt} = 0$  yields a first approximant:

$$w_X^{(1)} = C_X u_X^{(1)}$$

with

$$C_X = \left( -\frac{C_{200} + C_{020}s_X^2 + C_{110}s_X}{C_{101} + s_X C_{011}} \right).$$

Substitution to the first and second of Eqs.(16) yields a *unique* non-zero first approximant for  $u_X$  and  $v_X$ :

$$u_x^{(1)} = -\frac{A}{B_x}, \quad v_x^{(1)} = \frac{A}{A_x}$$

with

$$\begin{aligned} A_X &= A_{020} + \frac{1}{s_X} (A_{110} + A_{011}C_X) + \frac{1}{s_X^2} (A_{200} + A_{002}C_X^2) \\ B_X &= B_{020}s_X^2 + B_{110}s_X + B_{200} + B_{002}C_X^2 + B_{101}C_X \quad . \end{aligned}$$

Starting with the approximant  $(u_X^{(1)}, v_X^{(1)}, w_X^{(1)})$  we can finally refine the solution for the stationary point, e.g. via successive Newton iterates. The key remark is that, due to (28), one finds that  $R_X = \sqrt{u_X^2 + v_X^2} = \mathcal{O}(V^{-1})$ , where  $V = \sqrt{V_u^2 + V_v^2}$ . Thus, the X-point remains in the neighbourhood of the nodal point only when the nodal point moves fast.

The hyperbolic character of the stationary ‘X-point’  $(u_X, v_X, w_X)$  can be established as follows: The equations of the flow (16) come from the general expression:

$$\left( \frac{du}{d\tau}, \frac{dv}{d\tau}, \frac{dw}{d\tau} \right)^T = \rho \nabla S, \quad (31)$$

where  $\rho \equiv G = \Psi\Psi^*$ ,  $S = \arctan[\Im(\Psi)/\Re(\Psi)]$ . Setting  $u = u_X + \xi$ ,  $v = v_X + \eta$ ,  $w = w_x + \zeta$  and linearizing Eqs. (31) we obtain:

$$\left( \frac{d\xi}{d\tau}, \frac{d\eta}{d\tau}, \frac{d\zeta}{d\tau} \right)^T = M \cdot (\xi, \eta, \zeta)^T, \quad (32)$$

where  $M$  is the  $3 \times 3$  variational matrix with elements given by:

$$M_{ij} = \left( \rho \frac{\partial^2 S}{\partial q_i \partial q_j} \right) \Bigg|_{q_1=u_X, q_2=v_X, q_3=w_X}, \quad i, j = 1, 2, 3$$

and  $q_1 \equiv u$ ,  $q_2 \equiv v$ ,  $q_3 \equiv w$ . The matrix  $M$  is symmetric, therefore all three eigenvalues  $\lambda_i$ ,  $i = 1, 2, 3$ , are real. Using now the expansion (16), we find

$$M = \frac{1}{G_X} \begin{pmatrix} Av_X \frac{\partial G_X}{\partial u_X} + \mathcal{O}_3 & -AG_X + Av_X \frac{\partial G_X}{\partial v_X} + \mathcal{O}_3 & \mathcal{O}_3 \\ AG_X - Au_X \frac{\partial G_X}{\partial u_X} + \mathcal{O}_3 & -Au_X \frac{\partial G_X}{\partial v_X} + \mathcal{O}_3 & \mathcal{O}_3 \\ \mathcal{O}_3 & \mathcal{O}_3 & \mathcal{O}_3 \end{pmatrix} \quad (33)$$

where  $G_X = G_2(u_X, v_X)$ , and  $\mathcal{O}_3$  denotes terms of order 3 in the variables  $(u_X, v_X, w_X)$  (while only second order terms are explicitly written in Eq.(33)). One can easily check that  $-AG_X + Av_x \frac{\partial G_X}{\partial v_X} = AG_X - Au_X \frac{\partial G_X}{\partial u_X}$ , i.e. the matrix in the r.h.s. of Eqs (33) preserves the symmetry of the full matrix  $M$  to the leading order. We then find:

$$\lambda_1 \lambda_2 = -A^2 + \mathcal{O}_1, \quad \lambda_3 = \mathcal{O}_1 \quad . \quad (34)$$

This implies that the linear stability character of the X-point is hyperbolic, containing at least one stable and one unstable eigendirections, while  $|\lambda_3| \ll \min\{|\lambda_1|, |\lambda_2|\}$ , provided that the distance  $d_X$  of the X-point from the nodal point is small. In fact, from the equations for the first approximant  $(u_x^{(1)}, v_x^{(1)}, w_x^{(1)})$  we find that  $d_X = \mathcal{O}(V^{-1})$ , where  $V$  is the velocity of the nodal point  $V = (V_u^2 + V_v^2)^{1/2}$ .

### E. X-line and construction of the 3-d quantum vortex

According to the analysis of the previous subsections, to every nodal point  $\mathbf{r}_0$  along a nodal line we can associate a single X-point with the properties mentioned in subsection II D. Using the notation of subsection II B, the position of the nodal point  $\mathbf{r}_0$  is parameterized in terms of the length parameter  $s$ , starting from an arbitrary ‘origin’  $O$  in the nodal line, through the continuous vector function  $\mathbf{r}_0(s) \equiv (x_0(s), y_0(s), z_0(s))$ . Let  $(u_X(s), v_X(s), w_X(s))$  be the local co-ordinates of the X-point associated with the nodal point  $\mathbf{r}_0(s)$ . Assuming, now, the co-ordinate representation (8) is adopted, the curve defined by the parametric relations:

$$\mathbf{r}_X(s) = \begin{pmatrix} x_X(s) \\ y_X(s) \\ z_X(s) \end{pmatrix} = \begin{pmatrix} x_0(s) \\ y_0(s) \\ z_0(s) \end{pmatrix} + \begin{pmatrix} n_x & n_y & n_z \\ b_x & b_y & b_z \\ t_x & t_y & t_z \end{pmatrix}^{-1} \begin{pmatrix} u_X(s) \\ v_X(s) \\ w_X(s) \end{pmatrix} \quad (35)$$

where  $(n_x, n_y, n_z)$ ,  $(b_x, b_y, b_z)$ ,  $(t_x, t_y, t_z)$  are the xyz-coordinates of the normal, bi-normal and tangent vectors  $\mathbf{n}(s)$ ,  $\mathbf{b}(s)$ ,  $\mathbf{t}(s)$ , is the ‘X-line’ associated with the nodal line  $\mathbf{r}_0(s)$ .

It is to be emphasized that, since the dynamical system (15) was defined around *a single* nodal point along the nodal line  $\mathbf{r}_0(s)$  (i.e. for one value of the parameter  $s$ ), the X-line  $\mathbf{r}_X(s)$  defined as in Eq.(35) gives a *unique invariant hyperbolic point* corresponding to the fixed value of  $s$ . However, all other points of the X-line *do not* form an invariant set in this particular co-ordinate system  $(u, v, w)$ . On the other hand, as shown in Appendix I, starting from the whole family of dynamical systems of the form (15), it is possible to construct a unique dynamical system in which the X-line becomes an exact, normally hyperbolic, invariant manifold of the flow. In this new system, each point along the X-line is itself invariant, thus the stable and unstable manifolds of the X-line are formed by the union of the stable and unstable manifolds of each of the X-points along the X-line.

Joining this analysis with the local analysis around nodal points, we arrive at the following picture, shown schematically in Figs. 4 and 5. The X-line’s stable and unstable

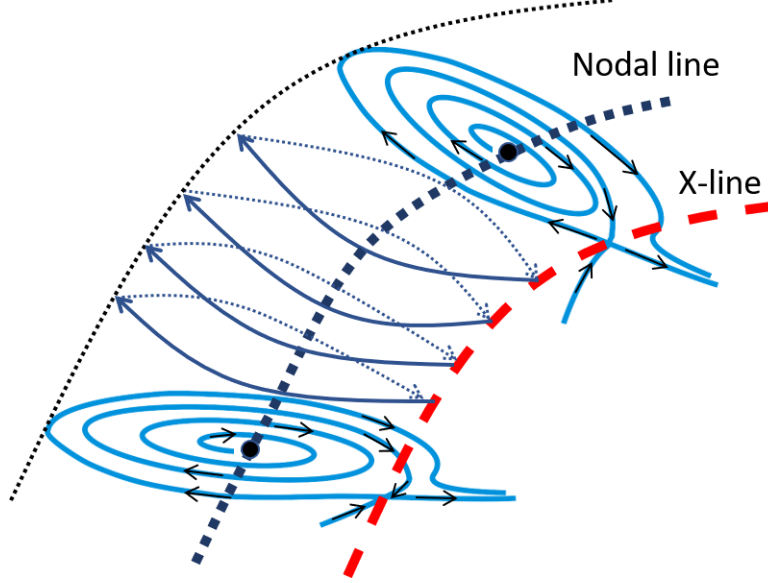


FIG. 4: Schematic illustration of a case in which one of the manifold branches from the X-line (foliation of all blue curves) terminates, after spiral-like revolution, at the nodal line (square dotted line in the center of the foliation).

manifolds ( $\mathcal{W}_X^S$  and  $\mathcal{W}_X^U$  respectively) are two-dimensional surfaces passing through the X-line. Depending on the values of the wavefunction coefficients (which change in time), one of the branches of either  $\mathcal{W}_X^S$  or  $\mathcal{W}_X^U$  continues as a spirally-twisting cylindrical surface which terminates at a second invariant set of the flow. In the simplest case, shown in Fig. 4, the manifold terminates in the nodal line. However, as noted in subsection IIC, Hopf bifurcations of limit cycles take place at every change of sign of the parameter  $\langle f_3 \rangle$  in Eq.(21). The value of  $\langle f_3 \rangle$  depends on the nodal point  $\mathbf{r}_0$  around which the wavefunction is expanded. Thus, Hopf bifurcations are possible to occur in time, for a specific moving nodal point, or in space, i.e., as we consider different nodal points in the nodal line at a fixed time  $t$ . Fig. 5 shows schematically the form of the cylindrical structure of NPXPCs in this latter case: the manifolds of some X-points are spirals terminating at a corresponding nodal point, while, for other X-points, the manifolds form spirals terminating at a limit cycle, while the spiral flow has opposite pitch angle inside each limit cycle.

Finally, the three remaining branches of the invariant manifolds of the X-line, which do not evolve as spirals, necessarily follow the nearby flow. One branch surrounds the whole cylindrical structure of NPXPCs, and then goes to infinity, while the remaining two branches extend from the start to infinity.

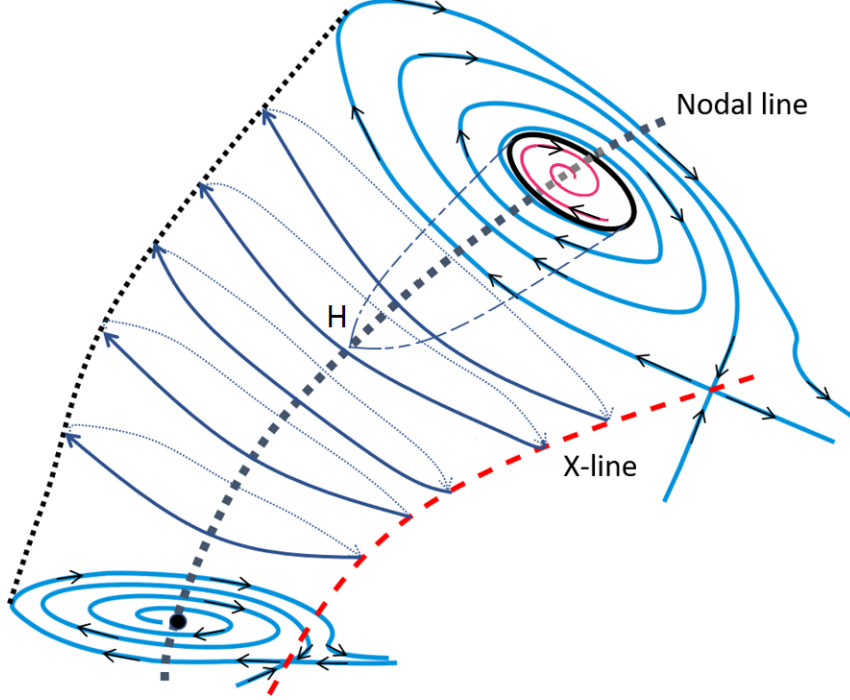


FIG. 5: Schematic illustration of a Hopf bifurcation taking place at the nodal point  $H$  of the nodal line (square dotted line in the center of the foliation). The bold closed curve in the upper section of the plot represents a limit cycle. Trajectories starting both outside or inside the limit cycle tend asymptotically to the latter in the forward or backward sense of time, depending on whether the limit cycle is attractor or repeller.

Precise computations of such complexes are hardly tractable, since explicit formulas for the associated dynamical system, in which  $\mathcal{W}_X^S$  and  $\mathcal{W}_X^U$  are to be constructed (see Appendix I), can only be given in approximative form. In practice, however, we can still use the approximation of a point-by-point approximation of these manifolds via the use of Eqs.(15) computed at different nodal points. Examples of this form are given in the next section.

Finally, we stress again that all critical sets and asymptotic manifolds defined in this and in previous subsections are invariants of the quantum flow only under the ‘frozen’ approach to the equations of motion (Eqs.14), i.e., only under the assumption that an adiabatic approximation holds, and that all Bohmian velocities within the NPXPCs are larger than the velocity  $V$  of the nodal point itself. Returning to the equations in the original time  $t$  without any approximation (Eqs. 13), at points of distance  $d$  from a nodal point the velocities are of order  $\mathcal{O}(d^{-1})$ . One thus gets that the adiabatic approximation holds in regions of size  $d < V^{-1}$ . Since the X-point is at a distance  $d_X \sim V^{-1}$ , the adiabatic approximation holds

for  $d < d_X$ . Hence, the outer limit of the cylindrical structure of NPXPCs marks at the same time the domain of validity of the adiabatic approximation. On the other hand, since the X-line is located at the border of this domain, the identification of the X-line as the main mechanism of hyperbolic scattering of the trajectories necessitates numerical validation. Such validation is provided by specific numerical examples in the section to follow.

### III. NUMERICAL APPLICATION

In this section we make a numerical application of the theory in the case of the wave function of 3-d harmonic oscillator:

$$\Psi(\vec{x}, t) = a\Psi_{p_1, p_2, p_3}(\vec{x}, t) + b\Psi_{r_1, r_2, r_3}(\vec{x}, t) + c\Psi_{s_1, s_2, s_3}(\vec{x}, t), \quad (36)$$

where  $\Psi_{n_1, n_2, n_3}(\vec{x}, t) = \Psi_{n_1, n_2, n_3}(\vec{x})e^{-iE_i t/\hbar}$  and  $\Psi_{n_1, n_2, n_3}(\vec{x})$  are eigenstates of the 3-d harmonic oscillator of the form

$$\Psi_{n_1, n_2, n_3}(\vec{x}) = \prod_{k=1}^3 \frac{\left(\frac{m_k \omega_k}{\hbar \pi}\right)^{\frac{1}{4}} \exp\left(\frac{-m_k \omega_k x_k^2}{2\hbar}\right)}{\sqrt{2^{n_k} n_k!}} H_{n_k}\left(\sqrt{\frac{m_k \omega_k}{\hbar}} x_k\right), \quad (37)$$

$n_1, n_2, n_3$  stand for their quantum numbers,  $\omega_1, \omega_2, \omega_3$  for their frequencies and  $E_1, E_2, E_3$  for their energies. Hereafter we set  $m_i = \hbar = 1$  and write  $x_1, x_2, x_3$  as  $x, y, z$ . For a given triplet of quantum numbers  $(n_1, n_2, n_3)$  we have  $E = \sum_{i=1}^3 (n_i + \frac{1}{2})\omega_i$ .

Chaotic trajectories scattered by the X-lines formed near moving nodal lines are typically found in systems of the form (36) (see, for example [45, 46]). As an application of the theory of section II we now focus on the case  $a = b = c = 1/\sqrt{3}$ ,  $p_1 = p_2 = p_3 = 0$ ,  $r_1 = r_3 = 1, r_2 = 0$ ,  $s_1 = 0, s_2 = 1, s_3 = 2$ , namely on the wavefunction

$$\Psi(\vec{x}, t) = \frac{1}{\sqrt{3}} \left( \Psi_{0,0,0}(\vec{x}, t) + \Psi_{1,0,1}(\vec{x}, t) + \Psi_{0,1,2}(\vec{x}, t) \right). \quad (38)$$

Figure (6) shows a real (non-schematic) computation of the 3-d cylindrical structure of NPXPCs in the system at the time  $t = 4$ . We observe the multiple nodal point-X-point complexes along the nodal line (black curve) and the red X-line which is the connection of X-points. Figure (7) shows a detail of Fig (6), i.e. a single nodal point X-point complex clearly depicting the invariant manifolds emanating from the X-point, and in particular the spiral motion around the nodal point.

The chaotic scattering effects in the neighborhood of the 3-d cylindrical structure of NPXPCs can be unravelled numerically as follows: in order to quantify chaos, we use as an indicator the local Lyapunov characteristic number, or ‘stretching number’ [48, 49]. If  $\xi_k$  is the length of the deviation vector between two nearby trajectories at the time  $t = \kappa t_0$ ,  $\kappa = 1, 2, \dots$ , the stretching number is defined as

$$\alpha_\kappa = \ln \left( \frac{\xi_{\kappa+1}}{\xi_\kappa} \right) \quad (39)$$

and the “finite time Lyapunov characteristic number” is given by the equation:

$$\chi = \frac{1}{\kappa t_0} \sum_{i=1}^{\kappa} \ln \alpha_i \quad (40)$$

The LCN is the limit of  $\chi$  when  $\kappa \rightarrow \infty$ .

Figure 8 shows a numerical investigation of the chaotic scattering effects close to the nodal line based on the use of Eqs.(39) and (40). The example shows a Bohmian trajectory in the system (38) for  $t \in [0, 20]$ , for which we compute the time evolution of the stretching number  $\alpha$ . The upper (red) curve shows  $\alpha$  as a function of time, while the middle (blue) curve shows the absolute value  $|\alpha|$  in a logarithmic scale, allowing to show more clearly weak scattering events. Finally the lower (black) curve shows the minimum distance between the trajectory and the X-line at every time  $t \in [0, 20]$ . This is done by projecting the trajectory to the closest nodal point of the nodal line corresponding to a given time  $t$ , and then calculating the X-point of the corresponding F-plane. This is an approximative method that simplifies the calculations, while still producing the key result with a satisfactory accuracy. Whenever a Bohmian trajectory comes close to one X-point of a 3-d structure of NPXPCs it gets scattered by it. At the same time the local Lyapunov exponent undergoes a jump and chaos is produced. The main effect, which depicts the cumulative mechanism of generation of chaos for the 3-d trajectory, is unraveled by comparing the times when jumps in the values of the stretching number appear with the times when the trajectory has its closest approaches to the X-line. These times appear to always coincide, while the largest jumps take place at distances  $d \ll 1$ . In fact, a careful inspection of the profile of the time evolution of the stretching number at every jump reveals profiles analogous in shape to those characterized as ‘type I’ or ‘type II’ in chaotic trajectories in the 2-d case (see [33]). Also, no jumps are observed when the trajectories are at distances  $d > 1$  from the X-line. This phenomenon

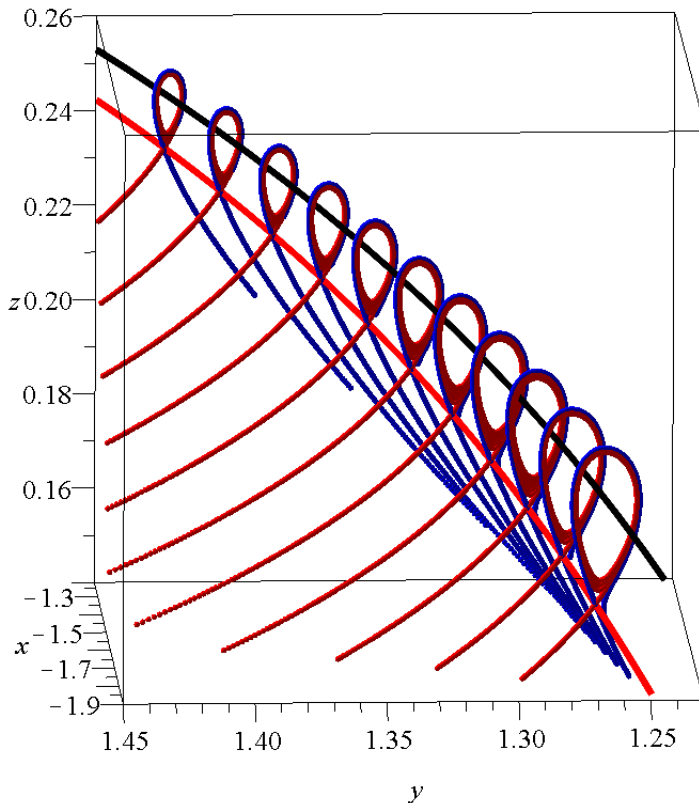


FIG. 6: Full numerically computed (non-schematic) example of the local quantum flow around a segment of a nodal line, leading to the formation of a 3-d structure of NPXPCs, in the case of the 3-d harmonic oscillator system described by Eq. (38) at the time  $t = 4$ . The black curve represents the nodal line. The red curve is the X-line, which connects the X-points of all complexes. The four branches of the stable (blue) and unstable (red) manifolds of the X-line are also plotted. One branch of the unstable manifold forms spirals surrounding and tending asymptotically to the nodal line.

is confirmed by repeating the computation of the local Lyapunov characteristic numbers in various trajectories in the same system, or in systems with different wavefunctions.

#### IV. CONCLUSIONS

In this paper we provide a general theory allowing to interpret the appearance of complex, or chaotic, behavior for quantum (Bohmian) trajectories tracing the quantum currents in 3-dimensional quantum systems. This theory extends results found in [33] from the 2-d to



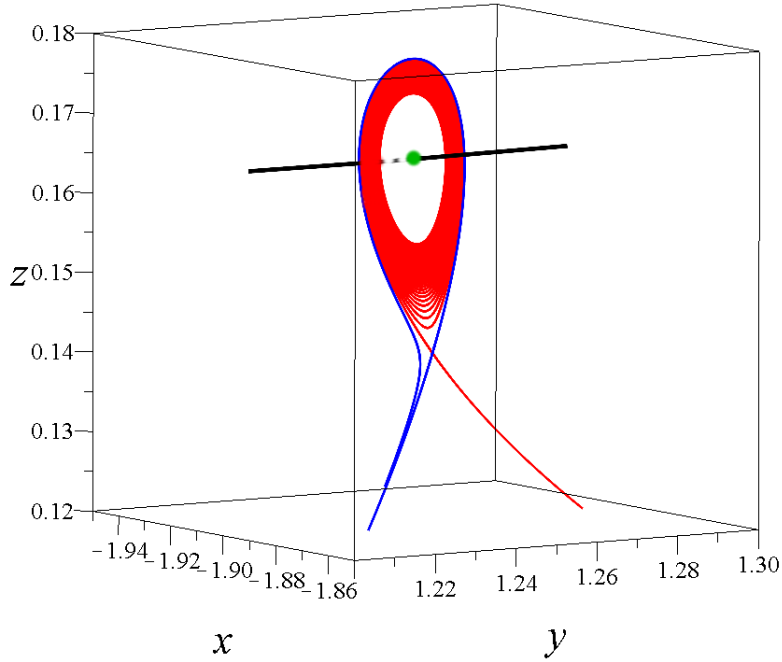


FIG. 7: Magnification of a single nodal point-X-point complex of the 3-d nodal point-X-point structure shown in Fig. 6.

the 3-d case, and it is based on general formulas which allow to characterize the form of the quantum flow in the vicinity of 3-d quantum vortices. In particular:

1. Starting from the analysis of [29], where it is shown that in the close neighborhood of a nodal line the quantum flow becomes stratified in planes orthogonal to the nodal line (here called the ‘F-planes’), we provide an analysis of the nonlinear terms in the equations of motion of trajectories tracing the quantum currents, as viewed in a frame of reference locally co-moving with every node along the nodal line. This analysis yields formulas derived by a generic second-order expansion of the wavefunction around nodal points, thus it applies to arbitrary 3-d wavefunctions  $\Psi$ .
2. As a consequence of symmetries identified in the transformed second order equations (which reflect the positiveness and preservation of quantum probability), we show that in the neighborhood of a time-evolving nodal line the quantum flow is spiral-helical, i.e., it describes spirals in the F-planes while drifting in a direction parallel to the nodal line. Approximative formulas are given which describe both the spiral motion

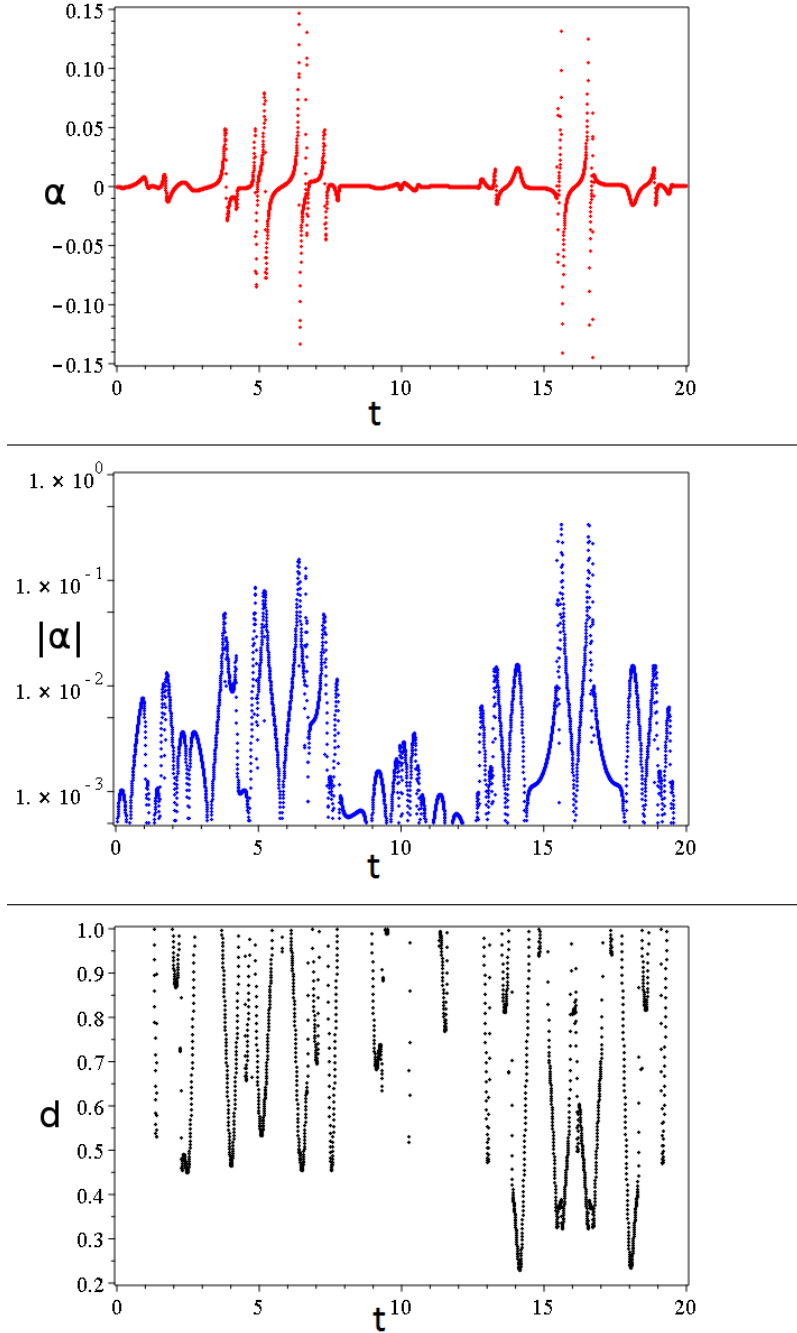


FIG. 8: Multiple scattering events for a Bohmian trajectory. The time evolution of the ‘stretching number’  $\alpha$  (upper panel), absolute value  $|\alpha|$  in logarithmic scale (middle panel), and minimum distance from the X-line (lower panel) are shown in the time interval  $0 \leq t \leq 20$ . The trajectory is computed in the model (36), with wavefunction (38), and initial conditions  $x(0) = -0.7, y(0) = -1.1, z(0) = 1.3$ .

and the drift. In particular, we define a crucial coefficient ( $\langle f_3 \rangle$ , see Eq.(22)), whose zeros describe Hopf bifurcations taking place both in time (the nodal line deforms as a whole), or in space (i.e. along a nodal line at a fixed time  $t$ ). Such bifurcations give rise to limit cylinders, which generalize the phenomenon of the bifurcation of limit cycles observed in [32].

3. Further away from a nodal line, we establish the existence of a normally hyperbolic one-dimensional curve called the ‘X-line’, whose three branches of manifolds extend to infinity, while one branch approaches asymptotically the nodal line by spirally revolving around it. The overall geometry of the quantum flow formed by the nodal line, the X-line and the latter’s asymptotic manifolds defines a ‘3-d structure of nodal point - X-point complexes’. We provide both schematic and real (numerical) examples of computation of such 3-d structures, and we examine their precise form depending on whether or not Hopf bifurcations take place along the nodal line. Finally, we argue that motion of the nodal line is a necessary condition for the X-line to be formed, as well as for the latter’s hyperbolic character.
4. We finally study the emergence of chaos in examples of trajectories computed fully numerically, i.e. without any analytical approximation of the equations of motion. We establish that the sensitivity to the initial conditions, quantified by the accumulation of positive values of the local Lyapunov Characteristic Numbers, is strictly correlated with close encounters of the trajectories with the X-line formed around every moving nodal line. The emergence of chaos through multiple scattering events of the trajectories with the X-lines is a generically observed behavior, in the sense that it appears for different initial conditions of the trajectories in the same quantum system, but also in systems with different (arbitrary) choice of 3-d wavefunction.

## ACKNOWLEDGMENTS

This research was supported by the Research Committee of the Academy of Athens.

## V. APPENDIX 1

Consider a segment  $\mathcal{S}$  of a nodal line  $\mathbf{r}_0(s)$  and a domain around  $\mathcal{S}$  defined by:

$$\mathcal{U} = \cup_{\text{all } s : \mathbf{r}_0(s) \in \mathcal{S}} \mathcal{V}_{\mathbf{r}_0(s), \epsilon(s)} \quad (41)$$

where  $\mathcal{V}_{\mathbf{r}_0(s), \epsilon(s)}$  denotes the domain  $\mathcal{V}_\epsilon$  defined in subsection II C for the nodal point corresponding to a specific value of  $s$ . Assume that the radii of curvature drawn from every point of  $\mathcal{S}$  do not intersect within  $\mathcal{U}$ . A curvilinear transformation  $(x, y, z) \rightarrow (U, V, S)$  can be defined within  $\mathcal{U}$  as follows: For every point  $P \equiv (x, y, z) \in \mathcal{U}$ : if  $P \in \mathcal{S}$ , set  $S = s$ ,  $U = V = 0$ , where  $s$  is the parameter value corresponding to  $P$ . If, now,  $P \notin \mathcal{S}$ , draw the normal from  $P$  to  $\mathcal{S}$ , which intersects  $\mathcal{S}$  at a certain point with parameter value  $s$ . Then, set  $S = s$ . Compute the normal and bi-normal vectors  $\mathbf{n}(s)$ ,  $\mathbf{b}(s)$ , and set  $U = xn_x + yn_y + zn_z$ ,  $V = xb_x + yb_y + zb_z$ .

We denote the above transformation as:

$$U = f_U(x, y, z), \quad V = f_V(x, y, z), \quad S = f_S(x, y, z) \quad .$$

Due to our adopted assumptions and domains, the functions  $f_U, f_V, f_S$  are smooth and invertible. The inverse functions are denoted by  $x = f_x(U, V, S)$ ,  $y = f_y(U, V, S)$ ,  $z = f_z(U, V, S)$ .

Take the complete Bohmian equations in the *inertial* frame (Eqs.(5)), and use the chain rule on the functions  $f_U, f_V, f_S$  and their inverses  $f_x, f_y, f_z$ . This allows to find the form that the equations (5) take in the new variables, resulting in the system:

$$\frac{dU}{dt} = F_U^{(inertial)}(U, V, S), \quad \frac{dV}{dt} = F_V^{(inertial)}(U, V, S), \quad \frac{dS}{dt} = F_S^{(inertial)}(U, V, S) \quad (42)$$

where the functions  $F_U^{(inertial)}, F_V^{(inertial)}, F_S^{(inertial)}$  are computed by applying the chain rule to both sides of Eq.(5).

Consider, now, a certain nodal point  $\mathbf{r}_0(s)$  and compute its associated X-point  $\mathbf{r}_x(s)$  (Eq.(35)). This is a new point with co-ordinates  $x_X, y_X, z_X$ . Use the transformation of the previous paragraph, and compute  $(U_X, V_X, S_X)$ . For every  $s$  we have a unique X-point, thus a unique value  $S_X$ . Thus, we can define a function  $s = \sigma(S_X)$ , which we assume to be smooth. Finally, the nodal point  $\mathbf{r}_0(s)$  has a velocity  $\mathbf{V}(s)$  defined by Eq.(7).

The following proposition is an immediate consequence of the above definitions: the dynamical system defined by

$$\begin{aligned}\frac{dU}{dt} &= F_U^{(inertial)}(U, V, S)_{t=t_0} - \mathbf{V}(\sigma(S)) \cdot \mathbf{n}(\sigma(S)) \\ \frac{dV}{dt} &= F_V^{(inertial)}(U, V, S)_{t=t_0} - \mathbf{V}(\sigma(S)) \cdot \mathbf{b}(\sigma(S)) \\ \frac{dS}{dt} &= F_S^{(inertial)}(U, V, S)_{t=t_0}\end{aligned}\tag{43}$$

possesses an exactly invariant X-line, which coincides with the one given by Eq.(35).

The quantities appearing in the r.h.s. of Eqs.(43) depend only on  $U, V, S$ , and they constitute the functions  $F_U, F_V, F_S$  of Eq.(2). In fact, by the above construction we can see that the Jacobian matrix of the system (43) is symmetric at any point along the X-line, thus its eigenvalues are real. Since every point on the X-line is invariant, one eigenvalue of the Jacobian matrix is necessarily equal to zero, and the corresponding eigenvector is tangent to the X-line. On the other hand, taking any arbitrary point on the nodal line as the origin O, the transformation  $(x, y, z) \rightarrow (U, V, S)$  differs from the one considered in subsection (II C), namely,  $(x, y, z) \rightarrow (u, v, w)$ , only by terms nonlinear in the quantities  $U, V, S$ . Thus, Eq.(34) still holds in the variables  $(U, V, S)$ . This implies that every point on the X-line is hyperbolic, hence, the X-line is a normally hyperbolic one-dimensional invariant manifold.

- 
- [1] A. Benseny, G. Albareda, Á. S. Sanz, J. Mompert, and X. Oriols, *Eur.Phys.J. D* **68**, 1 (2014).
  - [2] J. O. Hirschfelder, A. C. Christoph, and W. E. Palke, *The Journal of Chemical Physics* **61**, 5435 (1974).
  - [3] P. A. Dirac, *Proc. Royal Soc. A* **133**, 60 (1931).
  - [4] A. L. Fetter and A. A. Svidzinsky, *J. Phys. Condens. Matter* **13**, R135 (2001).
  - [5] A. S. Sanz and F. Borondo, *Eur. Phys. J. D* **44**, 319 (2007).
  - [6] D. Babyuk and V. Nechiporuk, *Rus. J. Phys. Chem. B* **5**, 730 (2011).
  - [7] C.-C. Chou, Á. S. Sanz, S. Miret-Artés, and R. E. Wyatt, *Phys. Rev. Lett.* **102**, 250401 (2009).
  - [8] R. P. Bell, *The tunnel effect in chemistry* (Springer, 2013).
  - [9] B. F. Curchod, I. Tavernelli, and U. Rothlisberger, *Phys. Chem. Chem. Phys.* **13**, 3231 (2011).
  - [10] S. Garashchuk, J. Jakowski, and V. A. Rassolov, *Mol. Simul.* **41**, 86 (2015).

- [11] S. Rudinsky, A. S. Sanz, and R. Gauvin, *J. Chem. Phys.* **146**, 104702 (2017).
- [12] Y. Atzmon and E. Shimshoni, *Phys. Rev. B* **85**, 134523 (2012).
- [13] R. Fazio and G. Schön, in *40 Years of Berezinskii–Kosterlitz–Thouless Theory* (World Scientific, 2013) pp. 237–254.
- [14] E. Madelung, *Zeit. Phys. A* **40**, 322 (1927).
- [15] D. Bohm, *Phys. Rev.* **85**, 166 (1952).
- [16] D. Bohm, *Phys. Rev.* **85**, 180 (1952).
- [17] C. Trahan and R. Wyatt, *Quantum Dynamics with Trajectories: Introduction to Quantum Hydrodynamics*, Interdisciplinary Applied Mathematics (Springer, 2005).
- [18] Á. S. Sanz and S. Miret-Artés, *A Trajectory Description of Quantum Processes. I. Fundamentals: A Bohmian Perspective*, LNP (Springer, 2012).
- [19] Á. Sanz and S. Miret-Artés, *A Trajectory Description of Quantum Processes. II. Applications: A Bohmian Perspective*, LNP (Springer, 2013).
- [20] E. Deotto and G. C. Ghirardi, *Found. Phys.* **28**, 1 (1998).
- [21] L. Vaidman, *Found. Phys.* **35**, 299 (2005).
- [22] D. Dürr and S. Teufel, *Bohmian mechanics: The Physics and Mathematics of Quantum Theory* (Springer, 2009).
- [23] S. Kocsis, B. Braverman, S. Ravets, M. J. Stevens, R. P. Mirin, L. K. Shalm, and A. M. Steinberg, *Science* **332**, 1170 (2011).
- [24] D. H. Mahler, L. Rozema, K. Fisher, L. Vermeyden, K. J. Resch, H. M. Wiseman, and A. Steinberg, *Sci. Adv.* **2**, e1501466 (2016).
- [25] N. Gisin, *Entropy* **20**, 105 (2018).
- [26] H. Wu and D. Sprung, *Phys. Rev. A* **49**, 4305 (1994).
- [27] H. Frisk, *Phys. Lett. A* **227**, 139 (1997).
- [28] H. Wu and D. Sprung, *Phys. Lett. A* **261**, 150 (1999).
- [29] P. Falsaperla and G. Fonte, *Phys. Lett. A* **316**, 382 (2003).
- [30] D. A. Wisniacki and E. R. Pujals, *Europhys. Lett.* **71**, 159 (2005).
- [31] D. Wisniacki, E. Pujals, and F. Borondo, *J. Phys. A.* **40**, 14353 (2007).
- [32] C. Efthymiopoulos, C. Kalapotharakos, and G. Contopoulos, *J. Phys. A* **40**, 12945 (2007).
- [33] C. Efthymiopoulos, C. Kalapotharakos, and G. Contopoulos, *Phys. Rev. E* **79**, 036203 (2009).
- [34] A. Cesa, J. Martin, and W. Struyve, *J. Phys. A* **49**, 395301 (2016).

- [35] C. L. Loprore and R. E. Wyatt, Phys. Rev. Lett. **82**, 5190 (1999).
- [36] D. Babyuk, R. E. Wyatt, and J. H. Frederick, J. Chem. Phys. **119**, 6482 (2003).
- [37] A. Alarcón, S. Yaro, X. Cartoixa, and X. Oriols, J. Phys. Condens. Matter **25**, 325601 (2013).
- [38] D. Marian, X. Oriols, and N. Zanghì, J. Stat. Mech. Theory Exp. **2016**, 054011 (2016).
- [39] E. Colomés, Z. Zhan, D. Marian, and X. Oriols, Phys. Rev. B **96**, 075135 (2017).
- [40] C. Efthymiopoulos, G. Contopoulos, and A. C. Tzemos, Ann. Fond. Louis de Broglie **42**, 133 (2017).
- [41] A. Valentini and H. Westman, Proc. Royal Soc. A **461**, 253 (2005).
- [42] C. Efthymiopoulos and G. Contopoulos, J. Phys. A **39**, 1819 (2006).
- [43] D. Dürr, S. Goldstein, and N. Zanghi, J. Stat. Phys. **68**, 259 (1992).
- [44] F. Borondo, A. Luque, J. Villanueva, and D. A. Wisniacki, J. Phys. A **42**, 495103 (2009).
- [45] A. C. Tzemos, G. Contopoulos, and C. Efthymiopoulos, Phys. Lett. A **380**, 3796 (2016).
- [46] G. Contopoulos, A. C. Tzemos, and C. Efthymiopoulos, J. Phys. A **50**, 195101 (2017).
- [47] S. Wiggins, *Normally hyperbolic invariant manifolds in dynamical systems*, Vol. 105 (Springer, 2013).
- [48] N. Voglis and G. Contopoulos, J. Phys. A **27**, 4899 (1994).
- [49] G. Contopoulos, *Order and Chaos in Dynamical Astronomy* (Springer, 2002).
- [50] S. H. Strogatz, *Nonlinear dynamics and chaos: with applications to physics, biology, chemistry, and engineering* (Hachette UK, 2014).